Published by IOP Publishing for Sissa Medialab

Received: *September 30, 2022*
Accepted: *October 20, 2022*
Published: *November 29, 2022*

23ND International Workshop on Radiation Imaging Detectors
26–30 June 2022
Riva del Garda, Italy

First demonstration of on-chip interpolation using a single photon counting microstrip detector

A. Bergamaschi,* M. Andrä,[1] R. Barten, F. Baruffaldi, M. Brückner, M. Carulla, S. Chiriotti, R. Dinapoli, E. Fröjdh, D. Greiffenberg, S. Hasanaj, J. Heymes, V. Hinger, P. Kozlowski, C.L. Cuenca, D. Mezza, A. Mozzanica, K. Moustakas, C. Ruder, B. Schmitt, D. Thattil and J. Zhang

Paul Scherrer Institute, Forschungsstrasse 111, 5232 Villigen PSI, Switzerland

E-mail: anna.bergamaschi@psi.ch

Abstract: Despite being used in many X-ray applications, hybrid single photon counting detectors are limited in spatial resolution due to the diffusion of the charge produced by single photons between neighboring electronic channels, also called charge sharing. In this work, we demonstrate that on-chip interpolation can be used to improve the effective spatial resolution in a single photon counting detector without increasing the number and density of interconnects between the sensor and the readout electronics. We describe a digital communication scheme between neighboring channels exploiting charge sharing to obtain a spatial resolution better than the channel pitch, which has been implemented for the first time in the MYTHEN III microstrip detector. The interpolation is achieved directly on-chip at the time the photons are absorbed, limiting the data throughput and the computational effort and allowing a higher photon flux compared to interpolation using analog detectors. Here we show the first results obtained with this interpolation mechanism, characterizing the spatial resolution in terms of modulation transfer function. The spatial resolution of the 50 µm pitch MYTHEN III microstrip detector can be improved from the 20 lp/mm given by the physical strip pitch to an average resolution of approximately 30 lp/mm using the interpolation method.

Keywords: Hybrid detectors; Si microstrip and pad detectors; X-ray detectors

*Corresponding author.

[1]Current affiliation at SOLEIL Synchrotron, L'Orme des Merisiers, Saint-Aubin — BP 48, 91190 Gif-sur-Yvette Cedex, France.

https://doi.org/10.1088/1748-0221/17/11/C11012

Contents

1 Introduction

Single photon counting hybrid detectors are widely used in many X-ray applications thanks to their ability to suppress the electronic noise, their virtually infinite dynamic range, fast frame rate, reliability, and ease of use [1]. Hybrid detectors consist of a segmented semiconductor sensor, where the X-ray radiation is absorbed, which is connected channel-by-channel to the CMOS readout electronics where the signal is amplified, filtered and digitized [2]. Microstrip detectors provide one dimensional information and usually rely on wirebonding interconnections between sensor and readout; pixel detectors produce 2D images and sensors and readout electronics are connected using bump-bonding. The yield of the interconnections between sensors and readout electronics is one of the challenges of hybrid detectors and their pitch is one the main limiting factors in the spatial resolution. The spatial resolution is also affected by the diffusion of the charge produced by the X-rays absorbed in the semiconductor sensor. The charge cloud drifts to the collecting electrode under the influence of a strong electric field applied to the sensor and is partially collected by neighboring electrodes. This effect is also referred to as "charge sharing".

In Single Photon Counting (SPC) detectors, the signal collected in the sensor electrode in is amplified, shaped, and counted as a photon only if it exceeds a user defined threshold. SPC detectors have virtually ideal performance in terms of Detective Quantum Efficiency (DQE) and dynamic range, and they are very easy to operate after accurate energy calibration. The threshold has to be properly set at 50% of the incoming photon energy and well above the electronic noise. However, when operated with a different threshold, the number of the counted photons can be wrong: if the threshold is below 50% of the incoming photon energy, a single photon can be counted multiple times in neighboring channels; if the threshold is too high or the charge is shared between more than two channels, the photon might be lost because its signal never overcomes the

2022 JINST 17 C11012

threshold in any of the channels [3, 4]. In particular, this can happen with a too high segmentation (small pixel or strip pitch) due to charge sharing.

1.1 Charge sharing

Charge sharing can be directly observed using segmented energy resolving detectors [5], while in single photon counting detectors it only has secondary effects which can be corrected with flat field normalization, but degrade the spectral and the spatial resolution of the detector [3, 6]. The effect of charge sharing can be described using a simple linear charge collection model [5]. Under this assumption, for microstrip detectors it is possible to obtain the ideal DQE of the detector by setting the comparator threshold at half of the photon energy. However, for pixel detectors, there will always be a region around the corners where the charge is shared between more than two pixels and none of them exceeds the 50% threshold level, also referred to as "corner effect" [4]. Additionally, in presence of a non-monochromatic continuous spectrum, charge sharing decreases the DQE in case of both pixel and microstrip detectors [7]. Charge sharing also causes a complex relationship between the threshold level and the Point Spread Function (PSF), i.e. the detector response to a point-like radiation source as a function of its position [7]. Even for microstrip detectors with the threshold correctly set at 50% of the photon energy, the PSF deviates from the ideal box function to a trapezium, due to the presence of the electronic noise degrading the spatial resolution [3].

A few single photon counting pixel detector projects developed some inter-pixel communication schemes in order to overcome the problem of charge sharing [8–10]. They mainly rely on charge summation between neighboring channels and they demonstrated an improvement of the spectral resolution and the DQE [11] and a reduction of the corner effect [6]. However, the charge summation increases the electronic noise and reduces the count rate capability of the detector.

It has been shown that when using a charge integrating detector with single photon resolution, charge sharing can be exploited to improve the spatial resolution of the detector beyond the strip or pixel pitch by interpolating between channels [12–14]. The interpolation algorithm is applied offline and converts the low resolution analog image into a high resolution digital image. However, it requires the detection of isolated photons and therefore a low photon flux ($\lessapprox 2E4$ ph/s/cm^{-2}) combined with a high data throughput in order to readout low occupancy images at a high frame rate.

These challenges motivate the development of on-chip interpolation schemes, which would be able to sustain higher photon fluxes and relax the requirements on the data backend. In this work we propose and characterize an on-chip solution to exploit charge sharing in order to improve the spatial resolution of SPC detectors.

1.2 The on-chip digital interpolation logic

Here we propose a simple interpolation scheme using only digital communication between neighboring channels. It has been first implemented in the MYTHEN III microstrip detector in one dimension (see section 2), but it could be extended to pixel detectors by using a more complex logic.

The system is based on two comparators and three counters per strip. The basic schematic of a channel is shown in figure 1. The High Threshold Comparator (HTC) is used to determine if a

2022 JINST 17 C11012

photon is absorbed in the strip and its threshold should always be set at 50% of the photon energy. The output of the Low Threshold Comparator (LTC) is routed to both neighboring channels and its threshold is set at a lower level to detect the presence of charge sharing. The three counters divide the strip in three regions and they will be called Central (CC), Left (LC) and Right (RC) Counters.

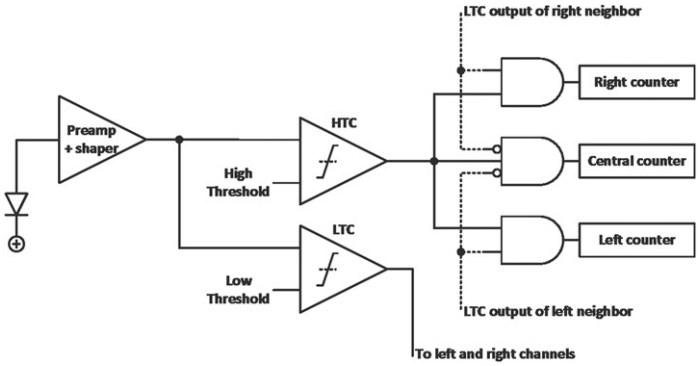

Figure 1. Schematics of the interpolation logic for one of the MYTHEN III channels. For simplicity, the logic defining the duration of the time window during which coincidences are evaluated is not drawn.

If the HTC fires, one of the counters of the strip will be incremented depending if the LTC of the neighbors fire during the time while the LTC of the counting channel is high. If the LTC of the left neighbors fires, the LC will be incremented; if the LTC of the right neighbor fires the RC will be increments; if none of the LTCs of the neighbors fire, the CC will be incremented.

The proposed method is very simple and can easily be implemented in every readout channel. However, it has no correction for double counts of a photon which can be assigned to both the LC and the RC due to the simultaneous arrival of one or more photons in the neighboring, or even next-neighboring strips. Moreover, the performance is strongly dependent on the threshold level of the LTC: higher levels will not allow the detection of charge sharing, while low levels too close to the noise floor can erroneously move counts from the CC to the LC or the RC due to the firing of the LTC of the respective neighbor due to a noise event.

Figure 2 shows the simulated PSFs for the three counters compared to the PSF without interpolation for a 50 µm pitch detector with 200 e^- ENC r.m.s. and 12 keV photons using a linear charge collection model with 30% charge sharing, which should be close to the expected performance of MYTHEN III. The dependence of the spatial resolution on the threshold of the LTC is clearly visible by comparing figures 2(a) and (b). The coincidence with noise from the neighbors at low LTC threshold levels is the reason for the reduction in the counts in the CC, and for the presence of the low counts plateau as wide as the whole strip in the case of the LC and of the RC (figure 2(b)).

When the width of the PSF of the LC and of the RC are much smaller than that of the CC, the adjacent RC and LC of two neighboring strips can be summed to obtain images with lower resolution but equally sized virtual pixels, which we will refer as Side Counters (SC). In order to estimate the overall resolution of the detector after interpolation, we also calculate the average PSF

2022 JINST 17 C11012

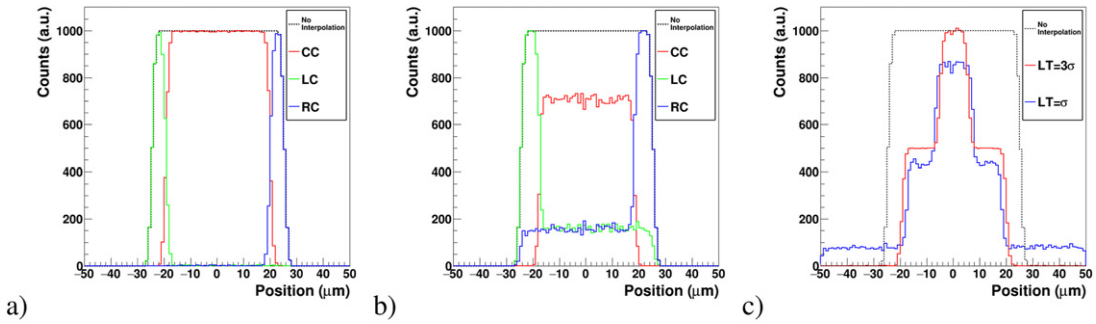

Figure 2. Simulated PSF (not normalized) in interpolation mode of a 50 µm pitch detector with 200 e^- ENC r.m.s. and 12 keV photons using a linear charge collection model with 30% charge sharing for the three counters with the low threshold value set at (a) 3 times the ENC (RMS) 3σ and (b) the ENC (RMS) level σ compared to the acquisition without interpolation. (c) PSF obtained by averaging the CC and the SC at two different low thresholds compared to the acquisition without interpolation.

(figure 2(c)), obtained by averaging the PSF of the CC and of the SC (the latter translated of 25 µm toward the center of the strip).

2 Materials and methods

MYTHEN III is a single photon counting microstrip detector mainly developed for powder diffraction experiments at synchrotrons. The readout chip contains 128 independent channels, each of which features a preamplifier and shaper with adjustable gain as well as three independent comparators with individual thresholds (global for the whole chip) and six trimbits per channel and per comparator, and three independently gateable 24-bit counters. MYTHEN III can be operated in different modes according to the kind of application. Depending on the operation mode, a counting logic distributes the counts towards the three counters in each channel. In this study we use the normal counting mode, exploiting a single comparator and the corresponding counter, and the interpolation mode described in section 1.2. In a module, a 1280 strips sensor is read out by 10 chips, which share the same analog biases and are controlled and readout in parallel using a 100 MHz clock. The frame rate of the detector can reach 300 kHz and dead-time-free acquisition is possible thanks to parallel counting and readout. A characterization of the detector and more details on the prototypes of the readout chip can be found in [15–17].

For this proof of concept experiment, MYTHEN III has been wirebondend to a standard 320 µm thick silicon sensor with 50 µm pitch, 8 mm long strips biased at 200 V. We have used 12 keV monochromatic photons with an approximate rate of 70 kHz per strip. The readout chip is configured with standard settings (shaping time ca. 100 ns). In order to calibrate the threshold value in energy units, s-curves have been acquired by scanning the comparator threshold (without interpolation). We applied consolidated methods to fit the s-curves and estimate the detector energy calibration parameters, electronic noise and charge sharing fraction [18]. For the settings used in this paper, we have measured an ENC = 140 ± 18 e^- r.m.s. and a charge sharing of 24 ± 4% (i.e. charge sharing happens in ca. 12 ± 2 µm, according to the linear charge collection model).

2022 JINST 17 C11012

The measurements presented in this study have been carried out at the SYRMEP beamline of the Elettra synchrotron radiation facility (Trieste, Italy) [19]. The MYTHEN III detector has been irradiated from backplane of the sensor as used in most experiments. For the imaging experiments at SYRMEP, the strips are oriented vertically with respect to the beam, such that only a fraction of each strip is illuminated. Moreover, the beam is shaped by means of ~15 µm wide slits to define the beam size in the strip direction.

3 Experimental results

3.1 Detector response

In interpolation mode, the response of the detector depends on both the HTC and the LTC threshold values. Figure 3(a) shows the S-curves acquired for the three counters scanning the HTC threshold at fixed 2.6 keV LTC value together with their sum, compared with the s-curve without interpolation mode. The sum of the three counters in interpolation mode is slightly shifted compared to the s-curve in normal mode, probably due to some baseline shifts introduced by the digital-to-analog crosstalk of the interpolation logic. As expected, the central counter starts oscillating when the LTC threshold value exceeds the HTC threshold. However, for larger HTC threshold values, the interpolation mode can be used to suppress charge sharing: the number of counts has almost no dependence on the threshold value and the detector behaves as if a collimator would be used to absorb the photons impinging between the strips, as it is often done in energy dispersive detectors to improve their energy resolution. This S-curve can be used as a golden standard to calibrate the detector in absence of charge sharing. By comparing the energy calibration using the central counter in interpolation mode and normal mode respectively, we observe a difference below 1% in terms of gain and offset, meaning that the phenomenological model that we use for fitting the detector S-curve can well determine the position of the inflection point, while the noise is overestimated by ~10% in normal mode. The left and right counters behave as expected very similarly, with small mismatches probably due to the remaining threshold dispersion unavoidable also after trimming.

When the high threshold is set at half of the photon energy, there is a small range of the LTC threshold value between ca. 2 keV and 4 keV which can correctly be used to redistribute for charge sharing detection as shown in figure 3(b). For LTC threshold levels lower than ~2 keV many counts are reassigned to the side counters due to noise counts in the neighbors, reaching almost 100% at ~1.8 keV (2.5 ENC). This is different from what is expected from simulations, where even at 1 ENC photons are counted in the CC. We attribute this difference to the fact that our simulations do not take properly into account the frequency behavior of the noise, but generate noise events only in coincidence with photons and cannot take into account the digital-to-analog cross-talk. For LTC threshold values higher than the HTC threshold, the HTC starts oscillating and the number of counts of the CC diverges to a fixed value depending on the time-over-threshold of the HTC.

When changing the HTC threshold (figure 3(c)), less counts are observed in the side counters at high thresholds, since only the photons absorbed in the center of the strip are detected. Changing the HTC threshold also affects the effective strip size [20].

2022 JINST 17 C11012

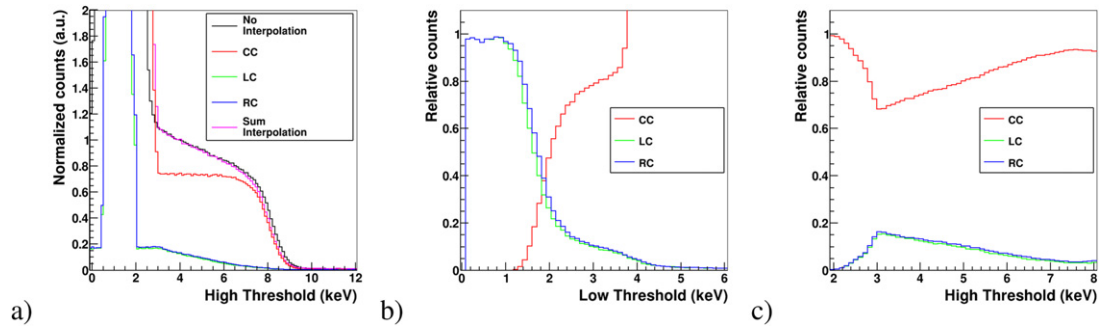

Figure 3. (a) Comparison of the S-curves obtained in interpolation mode with the low threshold set at 2.6 keV, with the S-curve acquired in normal mode using 8 keV copper fluorescence. Relative counts for the three counters in interpolation mode for one channel of the detector (b) with the high threshold set at 4 keV and changing the low threshold (c) with the low threshold set at 2.6 keV and changing the high threshold.

3.2 Spatial resolution

In order to quantitatively evaluate the spatial resolution of the detector, a tungsten edge aligned parallel to the strip direction is scanned in front of the detector. This allows to acquire an Edge Spread Function (ESF) i.e., the integral of the PSF for each strip/counter of the detector [21]. Since the different counters present very different PSFs (see figure 2), the ESF must be fitted with different functions which better resemble the integral of the various PSFs. The ESF for the normal counting mode and the CC are fitted with the integral of a box function; the ESF of the LC and of the RC are fitted with the integral of two box functions with different positions; the ESF of the sides counters (sum of LC and adjacent RC) is fitted with the integral of two box functions centered in the same position; the average ESF is fitted with the integral of three box functions centered in the same position. Figure 4(a) shows the measured ESFs and the resulting fits.

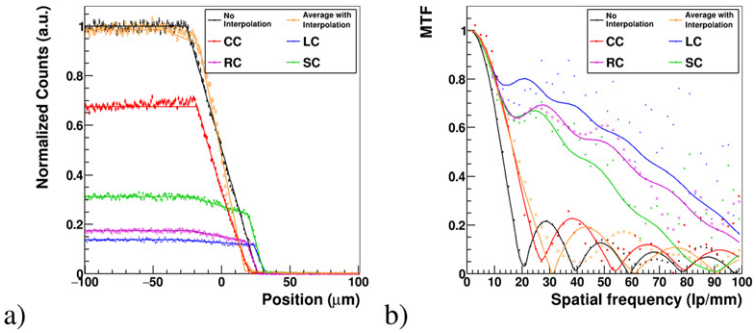

Figure 4. (a) Acquired image of a tungsten edge scanned in front of the strips and corresponding fits, and (b) resulting MTF. In both plots the markers are the raw data, while the solid lines are the fitted functions and their resulting Fourier transforms in the MTF plots.

2022 JINST 17 C11012

Figure 4(b) shows the Modulation Transfer Function (MTF) i.e., the Fourier transform of the PSF, which is a common figure of merit for the spatial resolution. Since the calculation of the derivative and Fourier transformed of the ESF are very sensitive to noise, we also plot the Fourier transform of the derivative of the fit of the ESF in order to quantitatively evaluate the data. It is evident that the first minimum of the MTF of the central counter is located at about 27 lp/mm compared to 20 lp/mm as defined by the physical strip pitch without interpolation. For the left and right counters, there is no big improvement in the spatial resolution at low spatial frequencies due to the value of the low energy threshold too close to the noise floor. However, both the MTFs of the LC and RC are still higher than 10% at 100 lp/mm. The MTF of the SC reaches the minimum at 90 lp/mm. The average MTF reaches the minimum at about 30 lp/mm, which is an improvement of about 50% in spatial resolution by using this interpolation method.

Unfortunately, the geometry of the sensor used in this study is not ideal to achieve an optimized spatial resolution using interpolation, since charge sharing takes place in only less than 25% of the strip area, and the average resolution is mainly determined by the FWHM of the CC. However, the spatial resolution can be optimized by varying several parameters which affect charge sharing i.e., the photon energy, the photon rate, the high and low threshold level, the detector settings, the sensor thickness and bias and the strip pitch. A more detailed characterization of the interpolation as a function of these parameters will be published in a future study.

3.3 Imaging

For a qualitative visualization of the effect of the interpolation mode on the spatial resolution, we imaged a sample consisting of a 2 µm thick golden Siemens star, with a diameter of 2 mm and an outer spike-pitch of 60 µm deposited on a 200 µm thick silicon wafer. The images were acquired at 12 keV in reference conditions (320 µm thick, 50 µm pitch, standard settings, 75 kHz count rate per strip). To acquire a two dimensional image, the Siemens star is scanned in front of the detector in 10 µm steps. The vertical resolution of the image is defined by the ~15 µm slit in front of the detector. Figure 5 compares the flatfield corrected images (a) without interpolation and (b) with interpolation using all 3 counters or (c) summing up the adjacent side counters. All counters have been plotted using the same pixel size, without rescaling for the effective width of the PSF.

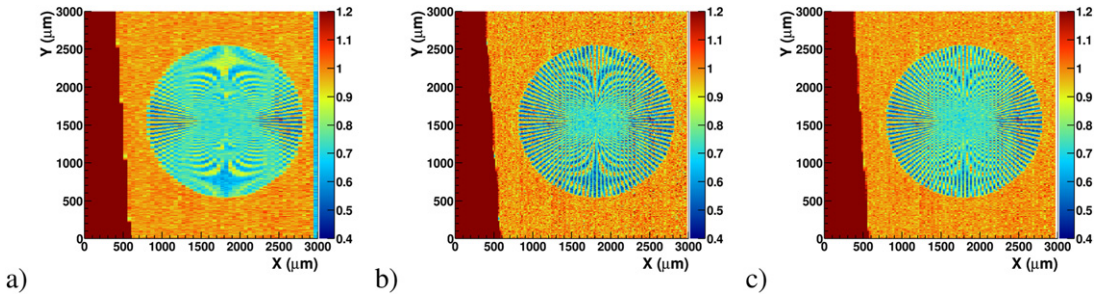

Figure 5. Image of a Siemens star with 60 µm external pitch acquired at 12 keV (a) without interpolation, (b) with interpolation using all counters and (c) with interpolation summing up the adjacent side counters after flatfield normalization. The sample is scanned vertically in 10 µm steps in front of a ca. 15 µm wide slit.

2022 JINST 17 C11012

While the vertical resolution is defined by the scanning step, there is an evident improvement in the horizontal resolution. The image using all three counters has a higher resolution (more spikes are visible), but when summing up the adjacent side counters the resolution is more uniform, as can be seen from the edge of the wafer on the left of the image. Both the interpolated images show flatfield related issues (vertical stripes), which need to be addressed by optimizing the low threshold value and eventually the photon flux.

4 Conclusion

This work is the first demonstration of an interpolation logic implemented in a single photon counting readout chip capable to exploit charge sharing to improve the spatial resolution. The results show an average improvement of about 50% in the spatial resolution, despite the non optimal geometry of the sensor used in this experiment. Energy dispersive spectrometers based on microstrip detectors could benefit by the improved spatial resolution while not being affected by the limitations in the detection rate which is an unavoidable disadvantage of inter-channel communication [22, 23]. The performance can further be improved by reducing the strip pitch to 25 µm or by replacing silicon with a high-Z sensors e.g. GaAs, where a large charge sharing is observed also with 50 µm pitch due to the longer charge collection time [24].

A similar interpolation logic can be modified to improve the spatial resolution of pixel detectors. However, additional complexity is required to cope with the corner effect: at least 4 counters (and up to 9) per pixel are required to improve the spatial resolution and more than 3 neighboring channels need to be connected. Moreover, the layout of the whole logic must fit in the pixel area, which requires a more advanced technological node than the 110 nm technology used for MYTHEN III. We expect that this study paves the way for high spatial resolution single photon counting detectors, based on a more advanced readout electronic rather than on smaller physical pixel sizes.

Acknowledgments

One of the authors (V. Hinger) has received funding from the European Union's Horizon 2020 research and innovation program under the Marie Skłodovska-Curie Grant Agreement No. 884104 (PSI-FELLOW-III-3i). The authors thank staff of the SYRMEP beamline of the Elettra synchrotron radiation facility (Trieste, Italy) for the support during the experiment.

References

[1] A. Förster et al., *A study of a natural population of Phytodecta olivacea (Forster) (Coleoptera, Chrysomeloidea)*, *Phil. Trans. R. Soc. A* **244** (2019) 205.

[2] L. Rossi et al., *Pixel Detectors — From Fundamentals to Applications*, Springer, Berlin (2006).

[3] A. Bergamaschi et al., *Performance of a single photon counting microstrip detector for strip pitches down to 10 µm*, *Nucl. Instrum. Meth. A* **591** (2008) 163.

2022 JINST 17 C11012

[4] F. Leonarski et al., *Fast and accurate data collection for macromolecular crystallography using the JUNGFRAU detector,* Nat. Methods **15** (2018) 799.

[5] A. Bergamaschi et al., *Looking at single photons using hybrid detectors,* 2015 *JINST* **10** C01033.

[6] E. Gimenez et al., *Study of charge-sharing in MEDIPIX3 using a micro-focused synchrotron beam,* 2011 *JINST* **6** C01031.

[7] J. Marchal, *Theoretical analysis of the effect of charge-sharing on the detective quantum efficiency of single-photon counting segmented silicon detectors,* 2010 *JINST* **5** P01004.

[8] R. Ballabriga et al., *The Medipix3 prototype, a pixel readout chip working in single photon counting mode with improved spectrometric performance,* IEEE Trans. Nucl. Sci. **54** (2007) 1824.

[9] P. Maj et al., *Algorithms for minimization of charge sharing effects in a hybrid pixel detector taking into account hardware limitations in deep submicron technology,* 2012 *JINST* **7** C12020.

[10] V. Di Trapani et al., *Characterization of the acquisition modes implemented in Pixirad-1/Pixie-III X-ray detector: effects of charge sharing correction on spectral resolution and image quality,* Nucl. Instrum. Meth. A **955** (2020) 163220.

[11] X. Ji et al., *Impact of anti-charge sharing on the zero-frequency detective quantum efficiency of CdTe-based photon counting detector system: cascaded systems analysis and experimental validation,* Phys. Med. Biol. **63** (2018) 095003.

[12] I. Ordavo et al., *A new pnCCD-based color X-ray camera for fast spatial and energy-resolved measurements,* Nucl. Instrum. Meth. A **654** (2011) 250.

[13] A. Schubert et al., *Micrometre resolution of a charge integrating microstrip detector with single photon sensitivity,* J. Synchrotron Radiat. **19** (2012) 359.

[14] S. Cartier et al., *Micrometer-resolution imaging using MÖNCH: towards G_2-less grating interferometry,* J. Synchrotron Radiat. **23** (2016) 1462.

[15] M. Andrä, PhD Thesis, ETH Zurich (2021).

[16] M. Andrä et al., *Towards MYTHEN 3: characterization of prototype chips,* Nucl. Instrum. Meth. A **936** (2019) 383.

[17] M. Andrä et al., *Towards MYTHEN III — prototype characterisation of MYTHEN III.0.2,* 2019 *JINST* **14** C11028.

[18] A. Bergamaschi et al., *The MYTHEN detector for X-ray powder diffraction experiments at the Swiss Light Source,* J. Synchrotron Radiat. **17** (2010) 653.

[19] G. Tromba et al., *The SYRMEP beamline of Elettra: clinical mammography and bio-medical applications,* AIP Conf. Proc. **1266** (2010) 18.

[20] F.C.M. Lopez et al., *Comparator threshold settings and the effective pixel width of the PICASSO detector,* 2014 *JINST* **9** C05056.

[21] E. Samei et al., *A method for measuring the presampled MTF of digital radiographic systems using an edge test device,* Med. Phys. **25** (1998) 102.

[22] E. Kleymenov et al., *Five-element Johann-type X-ray emission spectrometer with a single-photon-counting pixel detector,* Rev. Sci. Instrum. **82** (2011) 065107.

[23] Z. Nemeth et al., *Laboratory von Hámos X-ray spectroscopy for routine sample characterization,* Rev. Sci. Instrum. **87** (2016) 103105.

[24] M. Ruat et al., *Photon counting microstrip X-ray detectors with GaAs sensors,* 2018 *JINST* **13** C01046.